Chapter 3

Relativistic Compact objects with Anisotropic

3.1 Introduction

The study of compact objects are important in theoretical Astrophysics to understand the physics of the matter at extreme conditions. The Equation of state (EoS) of matter in a compact object is also not known clearly. These objects can only be studied by relativistic approach at present. In relativity Einstein Field equations determines the dynamical and statistical aspects of objects. For stars having nuclear matter density the EoS of matter may be predicted from Einstein field equation prescribing a suitable geometry. In this direction Vaidya and Tikekar obtained different solutions of Einstein's field equations assigning different geometries with physical 3-spaces which have been reported in the literature [30, 48, 55, 60, 61]. Generally a polytropic equation of state (EOS) is used to describe a white dwarf or a less compact star [17]. During the last couple of decades it has been realized that a deviation from local isotropy in the interior pressure may originate in a compact star. It is known [18, 19, 20] that at very high enough densities with smaller size the anisotropic pressure plays an important role in determining stellar properties. The physical situations where anisotropic pressure may be relevant are very diverse for a compact stellar object [18, 19, 21, 22]. By anisotropic pressure we mean the radial component of the pressure (p_r) different from that of the tangential pressure p_t. the configuration leads to simple easily accessible physically viable models of such stars. For stars having nuclear matter density the EoS of matter may be predicted from Einstein field equation prescribing a suitable geometry. As discussed earlier Vaidya and Tikekar obtained different solutions of Einstein's field equations assigning different geometries with physical 3-spaces in the literature [30, 48, 55, 60, 61]. Pant-Sah [50] obtained a class of relativistic static non-singular analytic solutions in isotropic form with a spherically symmetric distribution of matter in a static space time which is found to lead to a physically viable causal model of neutron star with a maximum mass of $4M_{\odot}$. A class of compact stellar models using Pant and Sah solution for a spherically symmetric space time is obtained by us considering anisotropic fluid star in hydrostatic equilibrium having mass and radius relevant for neutron stars [57]. An alternative approach (Synge approach) by first making an *ad hoc* choice of the geometry and then exploration of the EOS for matter is followed here.

3.2 Anisotropic Compact Star Models

We consider a spherically symmetric static cold compact star in hydrostatic equilibrium described by the line element eq.(2.1). The interior matter is anisotropic which is described by

$$T^{\mu}_{\mu} = diag\ (\rho, -p_r, -p_\perp, -p_\perp) \tag{3.1}$$

where ρ, p_r and $p_\perp$ are energy density, radial pressure and transverse pressure respectively. Using the space time metric given by eq.(2.1), the Einstein's field eq.(1.1) in four-dimensions leads to the following equations :

$$\rho = -e^{-\mu}\left(\mu'' + \frac{\mu'^2}{4} + \frac{2\mu'}{r}\right) \tag{3.2}$$

$$p_r = e^{-\mu}\left(\frac{\mu'^2}{4} + \frac{\mu'}{r} + \frac{\mu'\nu'}{2} + \frac{\nu'}{r}\right) \tag{3.3}$$

$$p_\perp = e^{-\mu}\left(\frac{\mu''}{2} + \frac{\nu''}{2} + \frac{\nu'^2}{4} + \frac{\mu'}{2r} + \frac{\nu'}{2r}\right). \tag{3.4}$$

Using eqs. eq.(3.3) and (3.4) the anisotropy of fluid ($\Delta = p_r - p_\perp$), is given by

$$\Delta = e^{-\mu}\left(\frac{\mu''}{2} + \frac{\nu''}{2} + \frac{\nu'^2}{4} - \frac{\mu'^2}{4} - \frac{\mu'}{2r} - \frac{\nu'}{2r} - \frac{\mu'\nu'}{2}\right). \tag{3.5}$$

eq.(3.5) is a second-order differential equation which admits a class of **new solution** with anisotropic fluid distribution given by

$$e^{\frac{\nu}{2}} = A_o\left(\frac{1 - k\alpha + n\frac{r^2}{R^2}}{1 + k\alpha}\right), \qquad e^{\frac{\mu}{2}} = \frac{(1 + k\alpha)^2}{1 + \frac{r^2}{R^2}} \tag{3.6}$$

where

$$\alpha(r) = \sqrt{\frac{1 + \frac{r^2}{R^2}}{1 + \Lambda\frac{r^2}{R^2}}} \tag{3.7}$$

with R, Λ, k, A_o and n are arbitrary constants. For $n = 0$, it corresponds to solution for isotropic stellar model obtained by Pant ans Sah [50]. In this work we consider non-zero n which permits an anisotropic pressure distribution of a star in hydrostatic equilibrium. Eq.(3.6) permits a relation amongst the parameters which is useful for obtaining stellar models. The allowed values of the parameters are determined using the physical conditions imposed on the stellar solution for a viable model. The geometry of the 3-space in the above metric is given by

$$d\sigma^2 = \frac{dr^2 + r^2(d\theta^2 + sin^2\theta d\phi^2)}{1 + \frac{r^2}{R^2}}. \tag{3.8}$$

Eq.(3.8) corresponds to a 3 sphere immersed in a 4-dimensional Euclidean space. Consequently, the geometry of physical space obtained at the $t = constant$ section of the space time is given by

$$ds^2 = A_o^2 \left(\frac{1 - k\alpha + n\frac{r^2}{R^2}}{1 + k\alpha} \right)^2 dt^2$$

$$-\frac{(1 + k\alpha)^4}{(1 + \frac{r^2}{R^2})^2} \left[dr^2 + r^2(d\theta^2 + sin^2\theta d\phi^2) \right]. \tag{3.9}$$

One obtains the pressure anisotropy in terms of the geometric parameter from eq.(3.5) which is given by,

$$\Delta = \frac{2n\frac{r^2}{R^2}(8\alpha(1 + \Lambda\frac{r^2}{R^2})^3 + k^2\alpha X + Y)}{\alpha^{3/2}(1 + \Lambda\frac{r^2}{R^2})^4(1 + k\alpha)^2(1 + n\frac{r^2}{R^2} - k\alpha)} \tag{3.10}$$

where $X = 8\Lambda^2\frac{r^6}{R^6} + 4\Lambda(1 + 5\Lambda)\frac{r^4}{R^4} + 12\Lambda - 4$, $Y = (15\Lambda^2 + 10\Lambda - 1)\frac{r^2}{R^2} + k(4 + 12\Lambda + 16\Lambda^2)\frac{r^6}{R^6} + 4\Lambda(5 + 7\Lambda)\frac{r^4}{R^4} + (15\Lambda^2 + 26\Lambda + 7)\frac{r^2}{R^2}$. The geometry of 3 - space obtained at $t = constant$ section of the space time metric given by eq.(3.6) incorporates a deviation in a spherical 3 space, k is a geometrical parameter measuring inhomogeneity of the physical space and n is related to the anisotropy. Pant and Sah obtained the solution corresponds to $n = 0$ and $k \neq 0$ [50]. In this chapter the physical properties of compact objects filled with anisotropic fluid ($n \neq 0$) is studied. Consequently we determine the values of R, Λ, k and A_o for a viable stellar model as permitted by the field equation. The exterior Schwarzschild line element is given by

$$ds^2 = \left(1 - \frac{2M}{r_o}\right) dt^2 - \left(1 - \frac{2M}{r_o}\right)^{-1} dr^2$$
$$-r_o^2(d\theta^2 + sin^2\theta d\phi^2) \tag{3.11}$$

where M represents the mass of spherical object. The above metric can be expressed in an isotropic metric form [56]

$$ds^2 = \left(\frac{1 - \frac{M}{2r}}{1 + \frac{M}{2r}}\right)^2 dt^2 - \left(1 + \frac{M}{2r}\right)^4 (dr^2 + r^2 d\Omega^2) \tag{3.12}$$

using the transformation $r_o = r\left(1 + \frac{M}{2r}\right)^2$ where r_o is the radius of the compact object. The Schwarzschild metric given by eq.(3.12) will be matched at the boundary with the interior metric given by eq.(3.11).

3.3 Physical properties of anisotropic compact star

Eq.(3.6) will be used in this section to study physical features of compact objects with anisotropy in a general way. The stellar models are obtained using the following prescription :

(1) In this model, a positive central density ρ is obtained for $\Lambda < \frac{4}{k} + 1$.

(2) The interior solution should be matched with the isotropic form of Schwarzschild exterior solution at the boundary of the star ($r = b$), *i.e.*,

$$e^{\frac{\nu}{2}}|_{r=b} = \left(\frac{1 - \frac{M}{2b}}{1 + \frac{M}{2b}}\right) \;\; ; \; e^{\frac{\mu}{2}}|_{r=b} = \left(1 + \frac{M}{2b}\right)^2 \tag{3.13}$$

(3) By knowing the radial distance where the pressure at the boundary vanishes (*i.e.,* $p_r = 0$ at $r = b$) the physical radius of a star (r_o). The physical radius is related to the radial distance ($r = b$) through the relation $r_o = b\left(1 + \frac{M}{2b}\right)^2$ [56].

(4) Using eqs.(3.6) and (3.12) the ratio $\frac{M}{b}$ is determined, which is given by

$$\frac{M}{b} = 2 \pm 2A_o\left(\frac{1 - k\alpha + ny^2}{\sqrt{1+y^2}}\right) \tag{3.14}$$

where $y = \frac{b}{R}$. In this work we consider only negative sign as it corresponds to a physically viable stellar model.

(5) The density inside the star should be positive i.e., $\rho > 0$.

(6) Inside the star the stellar model should satisfy the condition, $\frac{dp}{d\rho} < 1$ for the sound propagation to be causal. To construct a viable stellar model we also consider that the usual boundary conditions *i.e.,* the first and second fundamental forms be made continuous across the boundary ($r = b$). Making use of the boundary conditions as mentioned above one determines the unknown parameter n, k, Λ and A_o which satisfy the criteria for a viable stellar model outlined above. The field equations are highly non-linear and intractable to obtain a known functional relation between pressure and density hence we adopt numerical technique. Imposing the condition that the pressure at the boundary vanishes, we determine y from (3.14). The square of the acoustic speed $\frac{dp}{d\rho}$ becomes :

$$\frac{dp}{d\rho} = -\frac{\sqrt{\alpha}(1 + k\sqrt{\alpha})(\xi_1 + \frac{\xi_2}{\sqrt{\alpha}} + \xi_3 + \xi_4)}{\xi_5} \tag{3.15}$$

where $\xi_1 = -4(-1+n+n^2+2n^2r^2+nr^4)(1+r^2\Lambda)^5 + 2\mathrm{k}^4(1+r^2)^4\Lambda(-1+3(3+2r^2)\Lambda)$

$$\xi_2 = 2k^3(1+r^2)^3((1+r^2)(\Lambda-1)\Lambda+$$

$n(1+(1+4r^2+2r^4)\Lambda-r^4\Lambda^2+r^4(3+4r^2+2r^4)^3\Lambda)),$

$$\xi_3 = k\sqrt{\alpha}(1+r^2\Lambda)^3(-2(-1+\Lambda-r^2\Lambda+r^2\Lambda^2)$$

$-n(-6+10\Lambda+8r^6\Lambda+4r^8\Lambda^2+r^2(-21+34\Lambda-5\Lambda^2)+r^4(-5+12\Lambda+\Lambda^2))+n^2(-8+4r^8(\Lambda-1)\Lambda-2r^2(9+7\Lambda)+r^6(5-26\Lambda+5\Lambda^2+r^4(3-52\Lambda+9\Lambda^2)))),$

$$\xi_4 = k^2(1+r^2)(1+r^2\Lambda)(-2(5+(4r^2-7-4r^4)\Lambda$$

$+(6+8r^2+19r^4+2r^6)\Lambda^2+r^4(-3+2r^2)\Lambda^3)+n^2(1+r^2)(4r^8(\Lambda-1)\Lambda^2-4-2r^2(3+5\Lambda)+r^6\Lambda(3\Lambda^2-5-6\Lambda)-r^4(1+16\Lambda+3\Lambda^2))+n(12-8\Lambda+12r^8\Lambda^3+4r^1\Lambda^3+r^2(42\Lambda-1-29\Lambda^2)+r^6\Lambda(5+2\Lambda+9\Lambda^2)+r^4(25\Lambda-3+3\Lambda^2-9\Lambda^3))),$

$$\xi_5 = 6(1+nr^2-k\sqrt{\alpha})^2(2\sqrt{\alpha}(1+r^2\Lambda)^5$$

$+k^3(1+r^2)^4\Lambda(-1+(3+2r^2)\Lambda)+2k^2(1+r^2)\sqrt{\alpha}(2+(3r^2-3-2r^4)\Lambda+(4+5r^2+13r^4)\Lambda^2+r^2(4+7r^2+13r^4+2r^6)\Lambda^3+r^6(r^2-1)\Lambda^4)+k(1+r^2)(6+(-5+16r^2-3r^4)\Lambda+(5+3r^2+33r^4-r^6)\Lambda^2+r^2(5+6r^2+27r^4+2r^6)\ \Lambda^3+(4r^8-2r^6)\Lambda^4)).$

The physical properties of anisotropic compact objects are studied numerically. From the condition that pressure vanishes at the boundary which follows from eq. (3.3), the size of a star is estimated for a given values of Λ and k. From eqs.(3.6) and (3.13), the compactification factor *i.e.,* mass to radius ratio $\frac{M}{b}$ of a star is determined which in turn determines the physical size of the compact star (r_o). The radius of an anisotropic compact object is obtained in terms of the model parameter R for a given set of values of the parameters Λ, A_o, k, n, and the mass (M). Thus for a known mass of a compact star R is determined which in turn determines the corresponding radius.

In figs. (3.1)-(3.4), the radial variation of pressure and density of anisotropic compact objects are plotted for different parameters. In figs. (3.1) and (3.2), variation of radial pressure is plotted for a given set of values of A_o, n and Λ for different k.The pressure increases with an increase in k whereas the density decreases. The central density also found to increase with decrease in the value of k. The radial variation of pressure with n is plotted in fig.(3.3). It is evident that although the pressure inside the star decreases with an increase in n, the density remains invariant. The radial variation of density with Λ is plotted in fig. (3.4). Both the density and the pressure are found to increase with an increase in Λ value showing an increase in corresponding central density. But the difference between central density with that of surface density reduces with increase in Λ. It is found here that both the pressure and the density are independent on A_o. The radial variation of pressure for different Λ is shown in fig. (3.5), it is evident that the decrease in radial pressure near the boundary is sharp for higher values of Λ. The variation of both radial and transverse pressure are plotted in fig. (3.6), it is found that the value of transverse pressure at the boundary is more than that of radial pressure although they begin with same central pressure at the centre. Fig. (3.7) is a plot of squared speed of sound *i.e.,* $\frac{dp}{d\rho}$ with different n values. It is found that $\frac{dp}{d\rho}$ is positive inside the star and obeys causality condition. It shows stability of the stellar models.

The reduced size of a star ($\tilde{b} = \frac{b}{R}$) is presented for different values of n and Λ in Table- 3.1,. It is observed that for a given Λ as n increases the reduced size of a star also increases. On the other hand, for a isotropic star as Λ increases for a given n the reduced size increases but in the case of an anisotropic star the reduced size decreases

Λ	$n = 0$	$n = 0.55$	$n = 0.58$	$n = 0.60$
4	0	0.333416	0.342962	0.34913
4.1	0.051703	0.332378	0.341709	0.347747
5	0.140301	0.323293	0.331121	0.336233
6	0.172643	0.314019	0.32075	0.325177
7	0.188117	0.305681	0.311647	0.31559
8	0.196376	0.298192	0.303591	0.307174
9	0.200904	0.291437	0.296399	0.299702
10	0.203298	0.285311	0.289924	0.293002

Table 3.1: Variation of $\tilde{b} = \frac{b}{R}$ for given $n = 0, 0.55, 0.58, 0.60$ with different Λ

Λ	$k = 0.60$	$k = 0.62$	$k = 0.63$
1	0.472227	0.497719	0.509691
2.5	0.423942	0.436794	0.442986
3	0.410826	0.422278	0.427808
4.5	0.38013	0.389138	0.393505
5.6	0.363177	0.371156	0.375029
6.1	0.356535	0.364154	0.367855
7.5	0.340542	0.347378	0.350702
8.3	0.332752	0.339243	0.342401
9.5	0.322458	0.328523	0.331477
10	0.318578	0.324491	0.327371

Table 3.2: Variation of reduced size $\tilde{b} = \frac{b}{R}$ with Λ for different k

in this case as one increases Λ. Reduced size of a star is tabulated for different k and Λ values in Table -3.2. It is evident that for a given Λ as we increase k the reduced size increases. However for a given k on increasing Λ the reduced size of the compact object decreases.

3.4 Physical Analysis

To obtain stellar model first we start with a compact object of known mass and estimate the radius of the corresponding compact object in terms of the geometric parameter R. In this case we consider compact objects with observed mass [15] that determines the radius of the star for different values of R that are permitted by a set of values of n, A_o, k and Λ. It is known that the radius of a neutron star is $\leq (11 - 14)$ km. [57], therefore, to obtain a viable stellar model for compact object the upper bound of the size is fixed accordingly. In the next section we consider three stars whose masses [15, 41, 62] are known from observations to explore suitability of the solutions considered here.

Model 1 : An X-ray pulsar Her X-1 [15, 31, 41] characterized by mass $M = 1.47\ M_{\odot}$, where $M_{\odot}$ = the solar mass we obtain a stellar configuration with radius $r_o = 8.311$ km., for $R = 8.169$ km. The compactness of the star in this case is $u = \frac{M}{r_o} = 0.30$. The ratio of density at the boundary to that at the centre for the star is 0.128 which is satisfied for the parameters $\Lambda = 1.9999$, $k = 0.641$, $A_o = 2$ and $n = 0.697$. It is found that compactness factor $u = 0.2$ accommodates a star of radius $r_o = 11.925$ km. which is within the limit of a neutron star. However, stellar models with different size and compactness factor with the above mass permitted

$\frac{M}{b}$	R in km.	Radius (r_o in km.)
0.3	8.169	8.311
0.28	8.574	8.828
0.26	9.048	9.424
0.25	9.317	9.757
0.20	11.096	11.925

Table 3.3: Variation of size of a star with $\frac{M}{b}$ for $k = 0.641$, $n = 0.697$, $\Lambda = 1.9999$ and $A_o = 2$.

	$\frac{\rho(b)}{\rho(0)}$	$\frac{\rho(b)}{\rho(0)}$	$\frac{\rho(b)}{\rho(0)}$
Λ	$n = 0.697$ $k = 0.641$	$n = 0.60,$ $k = 0.63$	$n = 0.50$ $k = 0.52$
1	0.449	0.508	0.633
1.1	0.447	0.505	0.619
1.2	0.444	0.502	0.607
1.3	0.444	0.498	0.597
1.4	0.436	0.494	0.589
1.5	0.432	0.490	0.580
1.7	0.429	0.475	0.565
1.9999	0.409	0.466	0.545

Table 3.4: Density profile $\frac{\rho(b)}{\rho(0)}$ of compact objects.

here are tabulated in Table- 3.3. It is also observed that as the compactness factor increases size of the star decreases. It is evident from the second column of Table-3.4 that increase in Λ value which is related to geometry lead to a decrease in the density profile of the compact object.

Model 2 : An X-ray pulsar J1518+4904 [15, 31, 41] characterized by mass $m = 0.72\ M_\odot$, where $M_\odot =$ the solar mass it is noted that it permits a star with radius $r_o = 4.071$ km., for $R = 8.169$ km. The compactness of the star in this case is $u = \frac{M}{r_o} = 0.30$. The ratio of its density at the boundary to that at the center is

$\frac{M}{b}$	R in km.	Radius(r_o in km.)
0.3	8.169	4.071
0.28	8.574	4.324
0.26	9.048	4.616
0.24	9.317	4.956
0.22	11.096	5.358

Table 3.5: Variation of size of a star with $\frac{M}{b}$ for $k = 0.63$, $n = 0.60$, $\Lambda = 1.1$ and $A_o = 2$.

0.142 which is obtained for values of the parameters $\Lambda = 1.1$, $k = 0.641$, $A_o = 2$ and $n = 0.60$. It is noted that a star of radius $r_o = 12.332$ km. results with same mass having lower compactness factor $u = 0.09$. It is evident from Table-3.5 that in this case as the compactness increases radius of the star decreases. The variation of density profile with Λ is tabulated in the 3rd column of Table -3.4. It is found that the density profile decreases as Λ increases.

Model 3 :For a compact object B1855+09(g) [15, 31, 41] characterized by mass $M = 1.6\ M_\odot$, where $M_\odot$ = the solar mass, it is noted that it permits a star with radius is $r_o = 9.047$ km., for $R = 8.169$ km. with compactness factor $u = \frac{M}{r_o} = 0.30$. The ratio of density at the boundary to that at the center for the star is 0.187 which is found for the values of the parameters $\Lambda = 1$, $k = 0.52$, $A_o = 2$ and $n = 0.50$. It is noted that a star of compactness factor $u = 0.22$ accommodates a star with radius $r_o = 11.907$ km. For the same mass considered here it is possible to obtain a class of stellar models with different size and compactness which are tabulated in Table-3.6. We note that radius of the star decreases with an increase in compactness. The variation of density profile with Λ is displayed in 4th column of Table- 3.4. It is observed that the density profile of the star decreases as Λ increases.

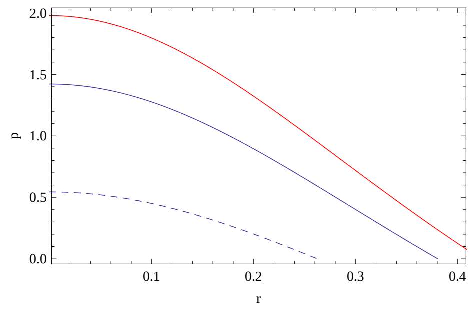

Figure 3.1: Radial variation of pressure for different k with $n = 0.60$, $\Lambda = 1.9999$ and $A_o = 2$. Red line for $k = 0.55$, blue line for $k = 0.5$ and dashed line for $k = 0.4$.

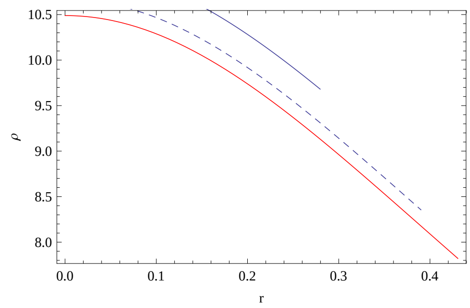

Figure 3.2: Radial variation of density for different k with $n = 0.60$, $\Lambda = 2$ and $A_o = 2$. Blue line for $k = 0.40$, dashed line for $k = 0.50$ and red line for $k = 0.55$.

3.5 Discussion

In this chapter, a class of new general relativistic solutions for compact objects which are in hydrostatic equilibrium considering an anisotropic interior fluid distribution is obtained. In the compact objects the radial pressure and the tangential pressure are found different which measures the anisotropy. As the EOS of the fluid inside a neutron star is not known so we adopt here numerical technique to predict EOS of the matter content inside the star for a given space-time geometry. The interior space-time geometry considered here is characterized by five geometrical parameters namely, Λ, R, k, A_o and n which are used to obtain different stellar models. For $n = 0$, the relativistic solution reduces to that considered in Refs. [50] and [63].

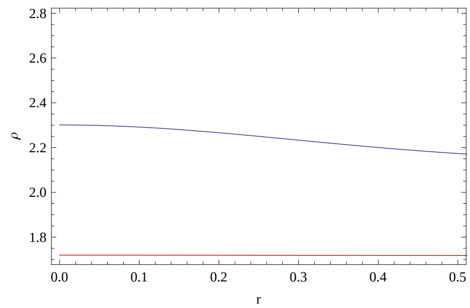

Figure 3.3: Radial variation of density for different Λ with $k = 0.641$, $n = 0.60$ and $A_o = 2$. Blue line for $\Lambda = 1.9999$, and red line for $\Lambda = 1.1$.

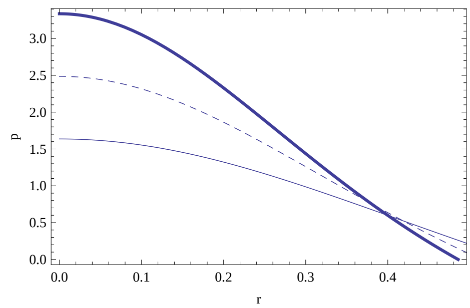

Figure 3.4: Variation of radial pressure for different Λ with $k = 0.641$, $n = 0.60$ and $A_o = 2$. Blue line for $\Lambda = 1.0$, dashed line for $\Lambda = 1.5$ and thick line for $\Lambda = 1.9999$.

$\frac{M}{b}$	R in km	Radius(r_o in km.)
0.3	8.169	9.047
0.28	8.574	9.609
0.26	9.048	9.818
0.24	9.317	11.013
0.22	11.096	11.907

Table 3.6: Variation of size of a star with $\frac{M}{b}$ for $k = 0.63$, $n = 0.60$, $\Lambda = 1.1$ and $A_o = 2$.

Star with mass	Radial pressure
HER X-1 $1.47M_\odot$	(i) $p_r = 1.207\rho - 8.477$ (ii) $p_r = 0.130\rho^2 - 1.032\rho + 0.980$
J1518+4904 $0.72M_\odot$	(i) $p_r = 1.041\rho - 7.607$ (ii) $p_r = 0.104\rho^2 - 0.794\rho + 0.350$
B1855+09(g) $1.6M_\odot$	(i) $p_r = 0.602\rho - 5.316$ (ii) $p_r = 0.043\rho^2 - 0.252\rho - 1.151$

Table 3.7: Variation of radial pressure with density for different stellar models.

The range of values of the unknown parameters are determined making use of the conditions : (i)interior metric matching at the boundary with the Schwarzschild metric. (ii) The square speed of sound :$\frac{dp}{d\rho} < 1$. (iii) pressure at the boundary is zero *i.e.,* $p = 0$ and (iv) positivity of density inside the star.

In figs. (3.1) and (3.2), the radial variation of pressure and density are plotted with three different k ($k = 0.4,\ 0.5,\ 0.55$) and $\Lambda = 1.9999$, $A_o = 2$, $n = 0.6$. It is evident that the radial variation of pressure increases with increase in k but the density decreases. The central density in all the three cases of the compact object is found to increase with decrease in k. In fig. (3.3), variation of radial pressure inside the star is plotted for different n. It is evident that pressure decreases as n increases, however density does not change. It implies that the anisotropy in this case does not affect the density of the compact object. In figs. (3.4) and (3.5), radial variation of density and pressure are plotted for different Λ. Both the pressure and the density in this case increases with an increase in Λ. The central density is also found to increase with an increase in Λ. The radial variation of pressure for different Λ is shown in fig.

(3.5). It is noted that the radial pressure near the boundary decreases sharply for higher values of Λ. The radial variation of anisotropy inside the star for different n, Λ and k are plotted in figs. (3.7), (3.8) and (3.9). It is evident that increase in Λ and n value permit a compact star with more anisotropy but increase in n permits a less anisotropic star. For a given Λ the reduced size of the star increases with increase in n. However for an isotropic star *i.e.,* $n = 0$ the size of a star increases with an increase in Λ which is tabulated in Table-3.1. We note that for non-zero values of n the size of the star decreases. The variation of size of the stars are tabulated in Table-3.2 it is evident that the size of the star increases as k increases for a given Λ, however, the size of star decreases as Λ increases for a given k. A class of compact stellar models with anisotropic pressure distribution are permitted with the new solutions obtained in this chapter. We consider three different compact objects with their observed masses, namely, HER X-1, J1518+4904 and B1855+09(g) to explore the physical properties of the star. The above mentioned stars can be fitted for different compactness factor exhibiting anisotropy that are evident in Tables-3.3, 3.5 and 3.6. The density profile of the models are also tabulated in Table- 3.4. The density profile inside the star is found to decrease as Λ increases. The functional relation of the radial pressure with the density for different stellar models considered here is presented in Table-3.7. It is noted that a viable stellar model may be obtained with a polynomial EOS. It is evident that both linear and quadratic EoS are possible to describe the interior matter. It may be mentioned here that similar EoS are considered recently in [64] and [65] to obtain relativistic stellar models. We note that though a stellar configuration in our case permits a linear EoS, it does not accommodate a star satisfying MIT bag model [65].

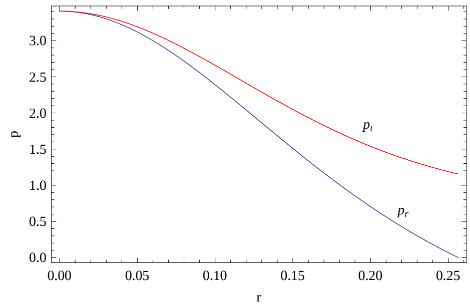

Figure 3.5: Radial variation of transverse and radial pressure with $\Lambda = 10$, $n = 0.8$, $A_o = 2$ and $k = 0.31$. Blue line for radial pressure and red line for transverse pressure.

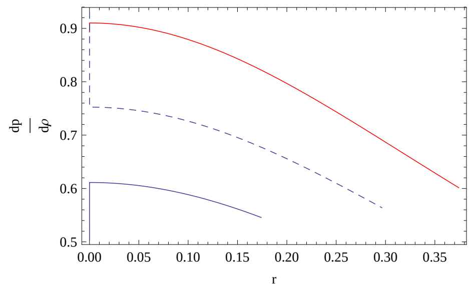

Figure 3.6: Radial variation of $\frac{dp}{d\rho}$ with different n for $k = 0.61669$, $\Lambda = 2$, $A_o = 2$. Red line for $n = 0.4$, dashed line for $n = 0.3$ and Blue line for $n = 0.2$.

It is also evident that the stellar models obtained here permit neutron stars with mass less than $2M_\odot$ for an anisotropic fluid distribution. The observed maximum mass of a neutron star is $2M_\odot$, therefore the stellar models obtained here may be relevant for compact objects with nuclear density. A physically realistic stellar model up to radius $(11 \sim 14)$ km. may be permitted here with the relativistic solutions accommodating less compactness [57]. The radial variation of the anisotropy measurement in pressure $i.e.$, Δ is plotted in fig.(3.10) with n. It is shown from the 3D plot that $\Delta \to 0$ when $n \to 0$ which leads to isotropic pressure case. For $n > 0$, the difference in tangential pressure to radial pressure initially increases which however attains a constant value for large n.

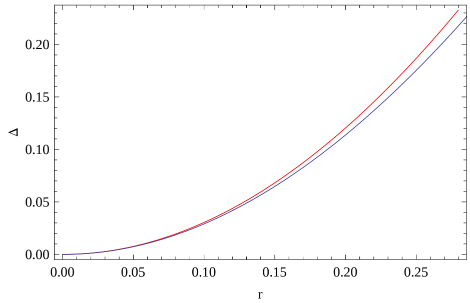

Figure 3.7: Radial variations of anisotropic parameter Δ for different n. Blue line for $n = 0.7$ and red line for $n = 1$.

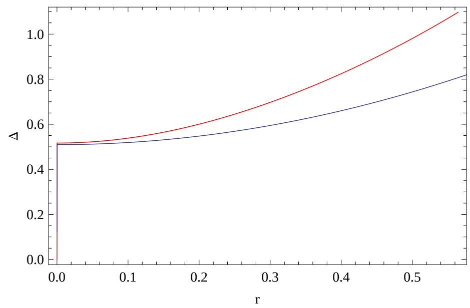

Figure 3.8: Radial variations of anisotropic parameter Δ for different Λ. Blue line for $\Lambda = 2$ and red line for $\Lambda = 5$.

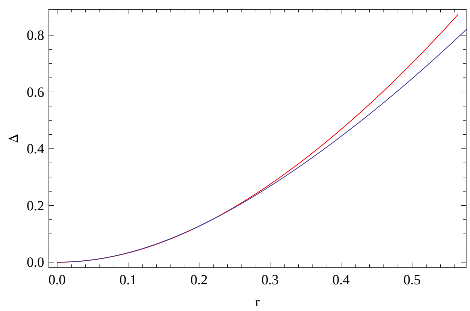

Figure 3.9: Radial variations of anisotropic parameter Δ for different k. Blue line for $k = 0.641$ and red line for $k = 0.52$.

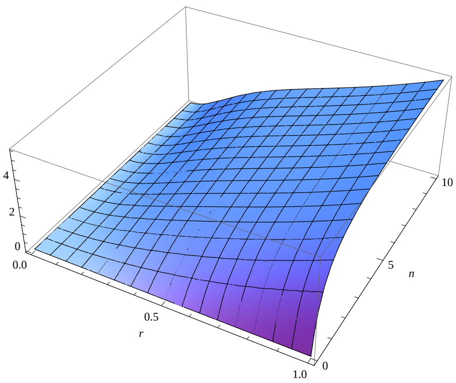

Figure 3.10: Plot of Δ with positive n and radial distance with $\lambda = 2$ and $k = 0.4$.